Journal of Statistical Physics, Vol. 39, Nos. 5/6, 1985

Generation and Detection of Propagating Solitons in Shearing Liquid Crystals[1]

Lin Lei,[2] Shu Changqing,[3] and Xu Gang[3]

Different methods of generating and detecting propagating solitons in uniform and nonuniform, steady and unsteady shearing nematic liquid crystals are proposed, reviewed, and discussed in detail. These include the use of (1) an external plate moving uniformly in the middle and at one end of the liquid crystal (LC) cell, (2) a LC cell with one glass plate moving uniformly and reversing in direction, (3) an external plate as in (1) but moving periodically, (4) pressure gradients along the long axis of the LC cell, (5) circular LC cell with one glass plate rotating, and (6) circular LC cell with radial pressure gradients. In each of these cases, the relevant equations of motion of the LC molecules are derived and analyzed. In the essentially one-deminsional cases of (1) to (3), the governing equation is the damped, driven since-Gorden equation. Analytic and numerical results of single and multisolitons are presented. A multiscale perturbation method is used in the unsteady case of (4). The related case of "soliton switch" in ferroelectric smectic C^* is discussed.

KEY WORDS: Liquid crystal; soliton; shearing; sine-Gordon equation; multiscale perturbation method; ferroelectric smectic C^*.

1. INTRODUCTION

In the ordered fluid of liquid crystals, because of the strong coupling of the director **n** (a unit vector representing the averaged local orientation of

[1] Invited paper presented at Conference on Transport and Propagation in Nonlinear Systems, Los Alamos, May 21–25, 1984.

[2] Department of Physics, City College, City University of New York, N.Y. 10031 (corresponding address); Department of Physics, Queensborough Community College, City University of New York, Bayside, New York 11364; and Institute of Physics, Chinese Academy of Sciences, Beijing, Chica.

[3] Institute of Physics, Chinese Academy of Sciences, Beijing, China.

0022-4715/85/0600-0633$04.50/0

molecules) with light, it is possible to observe the motion of the molecules and the solitons rather directly.[1,2]

Early discussions on solitons ("walls") in liquid crystals were due to Helfrich,[3] deGennes,[4] Brochard,[5] and Leger.[6] Subsequently, static solitonlike splay-bend distortions of nematics in a glass tube was discussed by Cladis and Kleman.[7] In Couette flow of nematic HBAB and CBOOA (in the regime $\gamma > 1$, see below) solitary waves were observed when "tumbling" instability occurred.[8] Also, small solitary vortices were seen propagating in the subcritical region of electroconvective instability by Ribotta.[9]

More recently, existence of static solitons ("discommensurations") in smectic A materials were proposed by Prost.[10] Walls in smectic C^* films and in nematics under electric field were treated by Pindak *et al.*,[11] Clark and Lagerwall,[12] and Carr and Kozlowski,[13] respectively. Condensation of solitons related to the transition between cholesteric and nematic phases in magnetic field was discussed by Yamashita *et al.*[14] Kinks were used to explain the large increase of the pitch in smectic C^* near the smectic-C^*–smectic-A transition.[15] In smectic C^* the transition between the two ferroelectric states with opposite polarization was observed to be mediated by solitary wave.[16] Walls in lyotropic nematics are discussed by Figuiredo Neto *et al.*[17] In the zig-zag patterns observed in electroconvective instabilities of nematics, ϕ^4 kinks are found.[18]

In this paper, the case of solitons in shearing nematics[1,2,19–21] is discussed. It represents an effort to study systematically the propagation of solitons in liquid crystals. These solitons are simple, propagating, easily controlled, and readily observable (even by the naked eye).

For completeness, we note that director waves have been linked to waves in biomembranches[22,23] (see footnote 4 in Ref. 2).[4]

2. SOLITONS IN UNIFORM STEADY SHEARING NEMATICS

2.1. Theory

For nematics with velocity $\mathbf{v} = (v(y), 0, 0)$ and $s \equiv \partial v/\partial y = \text{const}$ the equation for $\mathbf{n} = (\sin\theta, \cos\theta, 0)$, $\theta = \theta(x, t)$ is given by[1,2] the damped, driven sine-Gordon equation

$$M\theta_{tt} = K\theta_{xx} - \gamma_1\theta_t + \tfrac{1}{2}s(\gamma_1 - \gamma_2\cos 2\theta) \tag{1}$$

or, in dimensionless form,

$$\bar{M}\theta_{TT} = \theta_{XX} - \theta_T + \partial U/\partial\theta \tag{2}$$

[4] See also S. Rowlands, *J. Biol. Phys.* **11**:117 (1983).

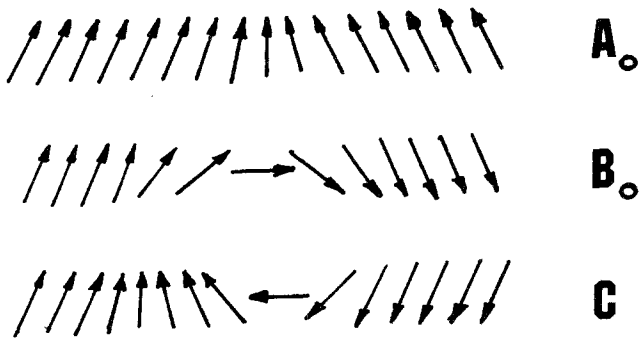

Fig. 1. Molecular orientations in three possible single solitons of Eq. (2) or (4). Shown here are A_0, B_0, and C types (see Table I for definitions).

with $U \equiv \gamma\theta + \frac{1}{2}\sin 2\theta$, $\bar{M} \equiv M/(\tau\gamma_1)$ (see Ref. 2 for notational definitions). For a traveling wave of velocity $\eta(>0)$, $\theta = \theta(X - \eta T) \equiv \theta(Z)$, (2) becomes

$$m\ddot{\theta} = -\eta\dot{\theta} - \partial U/\partial\theta \tag{3}$$

For $\gamma \equiv \gamma_1/|\gamma_2| < 1$ the two steady uniform solutions of (2), $\theta = \theta_0$ and $\theta = -\theta_0$, are stable and unstable, respectively $[\pi/4 < \theta_0 \equiv \frac{1}{2}\cos^{-1}(-\gamma) < \pi/2]$. Solitons[5] are formed by connecting these two states (or their equivalents) in different ways (Fig. 1). As seen from (3), these correspond

[5] The word "soliton" used here and in Refs. 1, 2 and 19 is synonymous to "solitary wave" (or "propagating front").

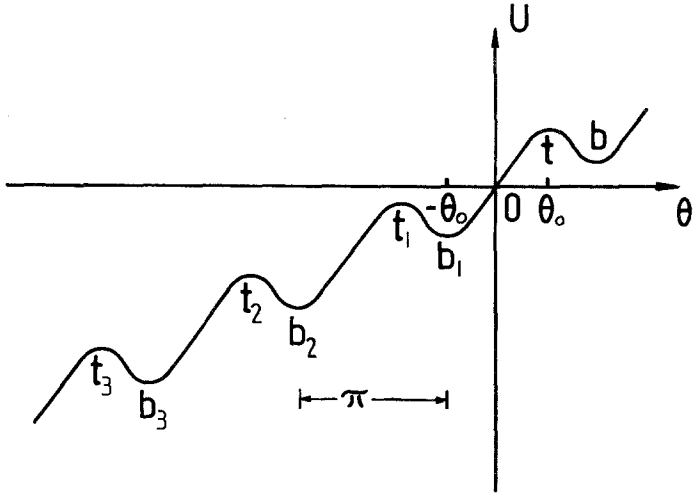

Fig. 2. Sketch of the fictitious potential U for $0 < \gamma < 1$.

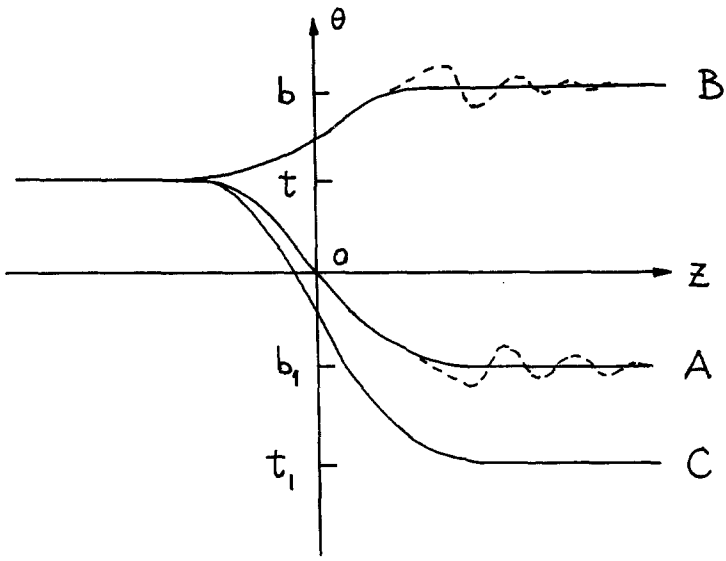

Fig. 3. Functional forms of the three types of solitons (A, B, and C). The solid curve of $A(B)$ is $A_0(B_0)$, the broken line is $A_1(B_1)$.

to a fictitious particle of mass m moving from a local maximum of U to its neighboring maximum or minimum (Figs. 2 and 3). There are four different types of single solitons (Table I). The case of $\eta<0$ is obtained by interchanging the asymptotic values of that for $\eta>0$ (Fig. 4). They are the antisolitons (which travel with negative velocities only, in contrary to the sG case).

Table I. Classification of Single Solitons ($\gamma<1$)[a]

Type	Mass m particle starts at	Mass m particle ends at	Condition of existence	With or without oscillating tail
A A_0	θ_0	$-\theta_0$	$\eta_a \leqslant \eta < \bar{\eta}$	No
A A_1			$\eta_c < \eta < \eta_a$	Yes
B B_0	θ_0	$(1/2)\pi-\theta_0$	$\eta_b \leqslant \eta < \bar{\eta}$	No
B B_1			$0<\eta<\eta_b$	Yes
C	θ_0	$\theta_0-(1/2)\pi$	$\eta=\eta_c$	No
D	θ_0	θ_0	$\eta=0$	No

[a] $\bar{\eta}=\bar{M}^{-1/2}$. All η's are functions of γ only. Upper and lower limits for η_a, η_b, and η_c are available.[20] $0<\eta_c<1.68$.

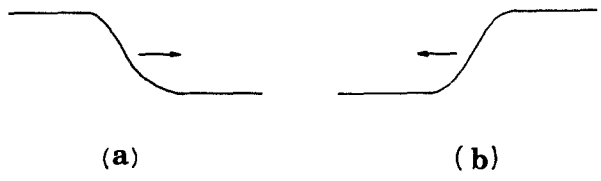

Fig. 4. (a) Soliton A_0 (or C). (b) Antisoliton $\bar{A}_0$ (or $\bar{C}$). They always move in oppsite directions.

In nematics (e.g., MBBA), $\bar{M} \sim 10^{-11}$. The θ_{TT} term in (2) is important in a transient time $T \sim \bar{M}^{1/2}$ in the beginning only.[20] Equation (2) is thus practically equivalent to

$$\theta_T = \theta_{XX} + \partial U/\partial\theta \tag{4}$$

which is a nonlinear diffusion equation[24] corresponding to the case of $m = 1$ in (3). The discussion above obviously applies to both (2) and (4).

The C soliton is linearly stable.[24] A_0 and B_0 solitons are marginally stable[25,26] (with respect to localized perturbation) which are physically relevant and observable.[2,27]

Analytic soliton solutions of (2) and (4) are available[2,19] for $\eta \gg 1$ (and for A_0 and B_0 types only). Computer calculations have been done, e.g., in Refs 20 and 26. The collision and annihilation of a $A\bar{A}$ pair is shown in Fig. 5.[20] In contrast to the sG case, they neither penetrate each other nor form a bound state (the breather) but end up as the stable state $\theta = \theta_0$.

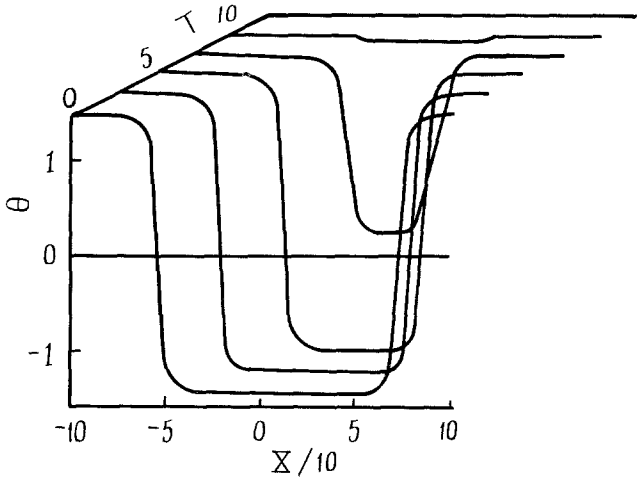

Fig. 5. Annihilation of $A\bar{A}$ soliton pair. $\gamma = 0.96$ ($\theta_0 = 1.42$).

The time evolution of multisolitons (which are not traveling waves) are also calculated. The cases of *CCA* and *CCC* are shown in Fig. 6. The local velocities η_i at $\theta = k\pi$ ($k = 0, -1, -2$) are plotted in Fig. 7. At large T, we see that in the *CCA* case, η_3 tends to a value much larger than η_2 ($\gtrsim \eta_1$), while in *CCC*, all η_i tend to a single value (at $T > 6$). This result may be understood as follows. In multisolitons, locally speaking, each part connecting two adjacent maxima will eventually (at $T \to \infty$) evolve into a C soliton (with velocity η_c) and the part connecting a maximum and an adjacent minimum wll evolve into an A_0 soliton (with velocity $\eta \geqslant \eta_a > \eta_c$). For $\gamma = 0.96$ and $M = 0$, $\eta_c = 1.32$ and $1.50 < \eta_a < 2.54$.[20] These values and the results in Fig. 7 are consistent with the above picture. The above conjucture of $\eta_i \to \eta_c$ at $T \to \infty$ for *CCC* is guaranteed by the theorems of Fife and McLeod[29] which holds for (4) only. The corresponding theorems for (2) ($M \neq 0$) and the case of *CCA* (with $M = 0$ or $\neq 0$) remain to be proved mathematically.

Apart from Ref. 29, the relevant theorems governing the emergence of solitons from arbitrary semilocalized initial data $\theta(X, 0)$ for the parabolic equation (4) are those of Aronson and Weinberger.[30] When applied to (4), for localized $\theta(X, 0)$ which is bounded in the region $[b_1, t]$, $[t, b]$, and

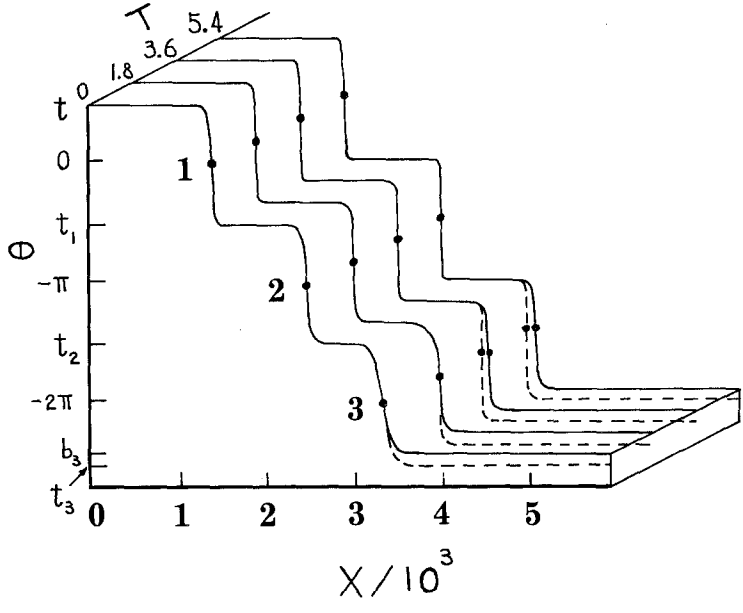

Fig. 6. Time evolution of two nultisolitons (solid line, *CCA*; broken line, *CCC*). The dots are at $\theta = -k\pi$, $k = 0, 1, 2$ (observable as dark lines under white light).

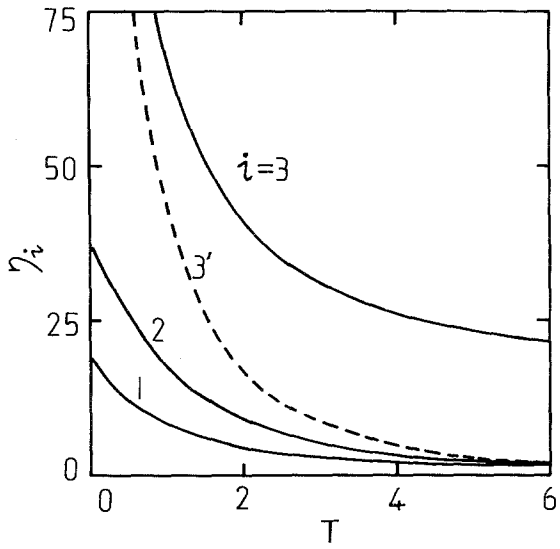

Fig. 7. Local velocity η_i corresponding to the dots in Fig. 6. η_1 and η_2 are the same for both *CCA* and *CCC* multisolitons. η_3 and $\eta_{3'}$ correspond to *CCA* and *CCC*, respectively.

$[t_1, t]$ (or equivalent ones obtained by a shift of a multiple of π; see Fig. 1), respectively, the emerging soliton at $T \to \infty$ is one with unique velocity η_a, η_b, and η_c in each case (corresponding to the A_0 and B_0 with minimal velocities and C, respectively). Note that, to our knowledge, there is no corresponding mathematical investigation of the hyperbolic equation (2).

Numerical calculations on this problem has been carried out by us.[31,32] The results are relevant to the problem of pattern selection.[26]

2.2. Experiments

To generate the above solitons in nematics, one must (i) create and maintain a uniform steady shear, (ii) generate the solitons by some means, and (iii) supply energy continuously to keep the solitons propagating.

One possible way to do this[33] is illustrated in Fig. 8. The pushing plate serves the purposes of (i) and (iii).[2] Point (ii) is less apparent. When the plate is being pushed some nematic must flow out of the cell in the opposite direction and a complicated (uncontrolled) initial state $\theta(X, 0)$ localized near the pushing plate is created. In our opinion, a multisoliton is generated resulting from the time evolution of this $\theta(X, 0)$ and is what has been observed by Zhu.[33] This conclusion is supported by the following results.

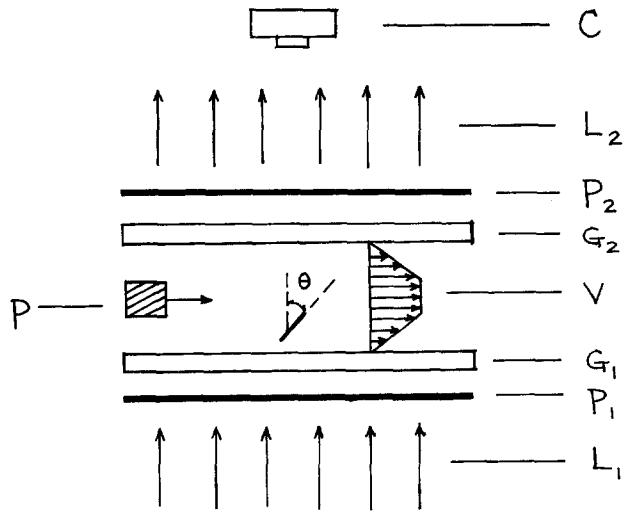

Fig. 8. Sketch of experimental setup of Ref. 33. The pushing plate (P) creates[2] a velocity profile (V) in the nematic sandwiched between two glass plates (G_1 and G_2). Incident light (L_1) enters normally to the cell which is placed between two polarizes (P_1 and P_2, with polarization direction at 45° to the long axis of the cell). The transmitted light (L_2) is recorded by the camera (C).

The ratio of the transmitted to the incident white-light intensities $I(X, T)/I_0$ is a function[19] of $\sin^2\theta(X, T)$. In Fig. 9, I/I_0 corresponding to $\theta(X, T)$ of the *CCA* multisoliton of Fig. 6 is shown. (Similar results are obtained for the *CCC* multisoliton.) The three dark lines represent the vertical molecules (with $\theta = k\pi$). For each T, the width of the dark line increases with X. Also, the width of each dark line decreases with T. These are exactly the characteristics shown in Fig. 1 of Ref. 33. Since the observed

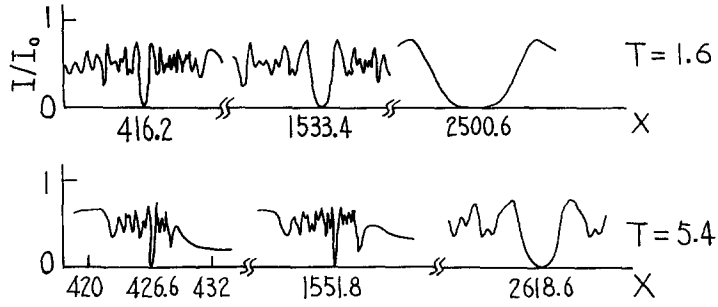

Fig. 9. Calculated transmitted white-light intensity I at $T = 1.6$ (the upper one) and $T = 5.4$ (the lower one) corresponding to the *CCA* multisoliton of Fig. 6. Same material parameters (for *MBBA*) as in Ref. 19 are used.

velocity of each dark line ($\eta_i \sim 10^2$–10^3)[2] is much larger than η_c and η_a we therefore identify[2] each dark line as an A_0 soliton (in the sense that each separated part of a multisoliton can be closely represented by a single soliton as in, e.g., the sG case). Note that the B soliton contains no vertical molecules and hence no dark line under white light. They cannot be observed with the set up of Ref. 33.

It should be pointed out that the deduction of $\theta(X, T)$ from $I(X, T)$ is not unique. For fixed T, the transmitted monochromaticlight pattern $I(X, T)$ consists of a series of dark lines.[2,19] For each such $I(X)$ with m *major* dark lines (i.e., those with $\theta = k\pi$, $k =$ integer, and show up as dark lines under white light) it can be proved[31] that there are 2^{m-1} different $\theta(X, T)$ corresponding to it. One can narrow this choice by noting the signs of the velocities of the major dark lines by comparing $I(X, T)$ with different T. In the case of three dark lines (under white light, i.e., $m = 3$) propagating in same direction observed by Zhu,[33] $\theta(X, T)$ should be[31] a monotonic decreasing function of X (such as those shown in Fig. 6).

In order to understand properly the mechanism of soliton generation in shearing nematics and to investigate the time evolution of $\theta(X, 0)$ experimentally it is important to start with a controlled $\theta(X, 0)$ (in contrast to Ref. 33). This may be achieved with the setup sketched in Fig. 10. The inner surfaces of the glass plates G, G_1, and G_2 are chemically treated as in a homeotropic cell (i.e., molecules perpendicular to plates at surfaces). Plate G is fixed. The (horizontal) velocities V_1 and V_2 of G_1 and G_2, respectively, can be varied independently at will. For example, if $V_1(t) = V_0$ ($=$const) and $V_2(t) = -V_0$ for $t < 0$ and $V_2(t) = V_0$ for $t > 0$, we will obtain (approximately) a $\theta(X, 0) = \theta_0$ for $X < X_0$ and $\theta(X, 0) = -\theta_0$ for $X > X_0$ and a uniform shear $s = V_0/d$ in the region $X > X_0$. The propagation of this $\theta(X, 0)$ into the $X > X_0$ region and the emerging soliton may by observed

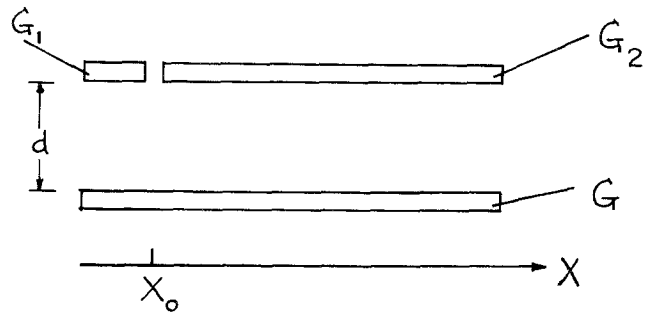

Fig. 10. Proposed experimental setup in generating solitons. Shown here is the liquid crystal cell in which the upper glass plate is split into two (G_1 and G_2) which can be sheared independently. The lower plate G is kept fixed. Crossed polarizers as in Fig. 8 should be included.

by transmitted light through crossed polarizers. It is advisable to use while light and monochromatic light simultaneously (by letting each one passing through half of the cell divided in the middle along the X axis) so that the position of the major dark line can be located in the white-light pattern while the monochromatic-light pattern provides more detailed information about $\theta(X, T)$. Experimentally, $I(X)$ for fixed T may be obtained through photographs of the transmitted light. Alternatively, $I(T)$ for fixed X may be measured by placing photocells at different locations along the cell. Different $\theta(X, 0)$ can be gnerated by using more complicated $V_1(t)$ and $V_2(t)$.[32]

3. SOLITONS IN UNIFORM UNSTEADY SHEARING NEMATICS

Let us consider the case of uniform unsteady shear such that $s = s(t)$ in (1). For slowly varying shear, $s = s(\varepsilon T)$, where ε is a small parameter. The corresponding diminsionless director equation is[21]

$$\bar{M}\theta_{TT} = \theta_{XX} - \theta_T + \bar{s}(\varepsilon T)\, \partial U/\partial\theta \tag{5}$$

Here $\bar{s} = s(t)/s_0$; s_0, the reference constant shear, is chosen such that $\bar{s}(0) = 1$; $\bar{M}$, X, and T differ slightly from those in Section 2 (in which $s_0 = s$). As in Section 2, $\bar{M}$ is small and practically vanishes.

The singular perturbation method of multiple scales is applied to this problem. The variables (X, T) are replaced by (ξ, ϕ) with $\xi \equiv \varepsilon T$ and $\phi = \phi(X, T)$ such that $\phi = X - C_0 T$ when $\varepsilon = 0$. $C_0 = \text{const} = \text{velocity}$ of traveling wave when $\varepsilon = 0$. $\theta = \theta(\xi, \phi)$ is expanded in a series,[6]

$$\theta = \theta_0(\xi, \phi) + \varepsilon\theta_1(\xi, \phi) + \varepsilon^2\phi_2(\xi, \phi) + \cdots \tag{6}$$

By eliminating the secular terms one obtains the equations governing θ_i. The final result, to order ε, is given by[21,34] $(C_0 \gg 1)$

$$\theta(X, T) = -\tan^{-1}\left(w \tanh\left\{(1-\gamma^2)^{1/2} C_0^{-1}\left[X - C_0\int_0^T \bar{s}(\varepsilon T)\, dT - X_0 - \varepsilon d_1 C_0\right]\right\}\right) \tag{7}$$

where X_0 and d_1 are constants and $w \equiv [(1+\gamma)/(1-\gamma)]^{1/2}$. When $\varepsilon = 0$ (7) reduces to the A_0 soliton with velocity C_0 of Section 2 [and is given in (4) of Ref. 2 with $\eta \equiv C_0$]. Similar results can be obtained for the B_0 soliton case.

[6] In (6), θ_0 is not the constant θ_0 in the rest of this paper.

Equation (7) describes a soliton with slowly changing velocity $C(t) = C_0\bar{s}(\varepsilon T)$, constant shape (in contrast to the KdV case[35]), and a phase shift proportional to ε. Numerical solutions of (5) are obtained[21] which agree with the analytic solution (7).

Experimentally, in the setup of Fig. 8, the pushing plate in the homeotropic MBBA cell has been given a periodic motion by Zhu[36] with frequency ω is the order of a few hertz. Under white light, three dark lines with time-varying velocities are observed. In our opinion, the periodic motion of the plate creates a uniform periodic shear profile (in the upper and lower parts of the cell shown in Fig. 8) approximately given by

$$s(t) = s_0 + s_1 \sin(\omega t) \tag{8}$$

In this case, $\varepsilon = \omega\tau$, $T = t/\tau$, $\tau \equiv 2\gamma/s_0$. The velocity of the dark line, with dimensions, is given by $c = C\lambda/\tau = C_0 s(t)\,\gamma^{-1}(K/2|\gamma_2|s_0)^{1/2}$. This dependence of c on the material parameters K, γ_2, and γ remains valid for the steady case of Section 2 (in which $s = s_0$ or $\omega = 0$). Note that the time-averaged velocity $\bar{c} = C_0\gamma^{-1}(s_0 K/2|\gamma_2|)^{1/2}$ is independent of ω. These prediction of (i) $c \propto s(t)$ and (ii) $\bar{c}$ independent of ω agree with the experimental results.[36] More detailed and precise experiments are needed for further checking of our theory.

A better experimental setup in generating arbitrary time-dependent shear is that proposed in Fig. 10. One can easily vary $V_2(t)$ periodically or in another fashion as one wishes [while keeping $V_1(t) = \text{const}$, say].

4. SOLITONS GENERATED BY PRESSURE GRADIENTS

To understand more thoroughly the generation mechanism of solitons and to find propagating solitons in other circumstances (other than those in Sections 2 and 3), experiments on nematic flow due to pressure gradients were carried out by Shu, Zhu, and Lin.[37,20] Pressures, P_1 and P_2, at two small holes near the two ends of a long homeotropic MBBA cell (size of each glass plates is $20 \times 5 \times 0.5$ cm) at room temperature (Fig. 11) can be

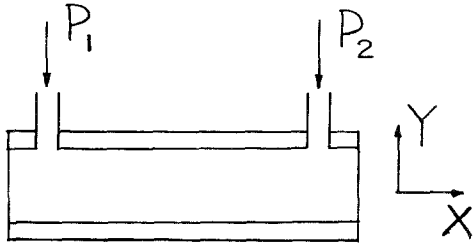

Fig. 11. Liquid crystal cell used in pressure-gradient experiments.[37,20] Thickness of the cell is 36 μm. Crossed polarizers (not shown here) as in Fig. 8 are used.

varied at will. Photographs of normally transmitted white and monochromatic lights (either separately or simultaneously; see Section 2) through crossed polarizers are taken. According to the time variations of P_1 and P_2, three different types of experiments were performed. The main results are summarized here.

4.1. Case A: Generation of One Single Soliton

The time variations of P_1 and P_2 are sketched in Fig. 12a. Under white light, at stage 1, the background is dark; at stage 2, this dark background is replaced gradually until entirely by a while background (no dark lines are observed); at stage 3, a single dark line (in contrast to three in Ref. 33) propagating from hole 1 to hole 2 is generated; at stage 4, a single dark line as in stage 3 is again observed.

Dark lines of different widths may be generated under the same conditions of P_1 and P_2 by using cells of different thicknesses. The velocity of

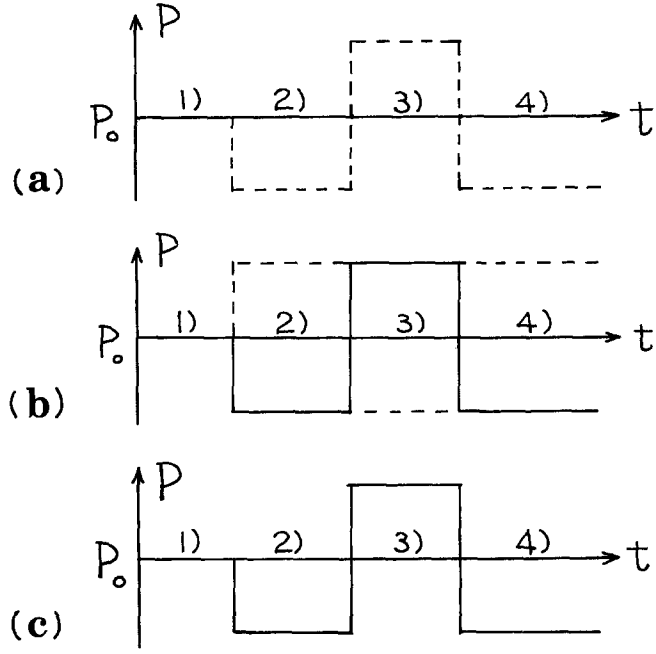

Fig. 12. Time variations of pressures P_1 and P_2 (defined in Fig. 11). Cases (a), (b), and (c) correspond, respectively, to the three types of experiments (A, B, and C) described in Section 4. In each case, there are four stages denoted by 1), 2), 3), and 4) in the diagram. Broken (solid) line represents P_1 (P_2). P_0 is atmospheric pressure. In all cases, $P_1 = P_2 = P_0$ at stage 1). In case (*a*), $P_2 = P_0$. In case (c), $P_1 = P_2$ (the solid curve).

the generated dark line is found to increase with its width (same as in Sections 2 and 3).

4.2. Case B: Collision and Annihilation of Two Solitons

P_1 and P_2 vary as in Fig. 12b. The observation at stages 1 and 2 are similar to Case *A*. At stage 3, two dark lines appear near the holes in the beginning and move head on toward each other. As they meet at the center of the cell, the dark lines disappear altogether. The same process repeats itself at stage 4.

4.3. Case C: Collision and Merging of Two Solitons

P_1 and P_2 vary as in Fig. 12c. Phenomena at stages 1 and 2 are similar to that in case A or B. At stage 3, two dark lines are generated and move as in case B, but when they meet they merge into one dark line instead. Same observation at stage 4.

Theoretical investigation of the above situations is due to Shu and Lin.[38] In contrast to Section 2, the shear $\partial v_x/\partial y$ is no longer constant and the problem is two dimensional in the (x, y) plane (y axis is normal of the cell). After appropriate simplifications, the effective dimensionless director equation of motion is

$$\theta_{XX}+\theta_{YY}-f(\theta)\theta_T+g(\theta)\,QY=0 \tag{9}$$

where $Q\equiv\partial P/\partial X$, P is the (dimensionless) pressure, and $f(\theta)$ and $g(\theta)$ are nonlinear even functions of θ depending also on the viscosities. A term $\bar{M}\theta_{TT}$ on the right-hand side of (9) is ignored. Boundary conditions are

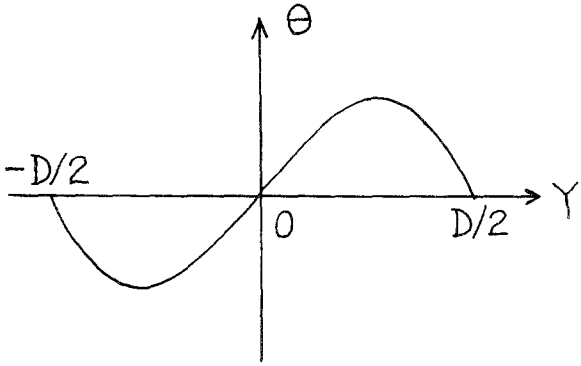

Fig. 13. Steady state solution, $\theta=\theta(Y)$, of Eq. (9) for $Q>0$. Q is pressure gradient along X direction. For $Q<0$, $\theta\to-\theta$.

$\theta = 0$ at $Y = \pm D/2$ (the two cell surfaces). Equation (9) admits the symmetries $\theta(X, -Y; Q) = -\theta(X, Y; Q) = \theta(X, Y; -Q)$. For $Q = \text{const} > 0$, the steady state of (9), $\theta = \theta(Y)$, uniform in X is obtained and depicted in Fig. 13. Solitary solutions, $\theta = \theta(Y, Z)$, $Z \equiv X - CT$, of (9) do exist and are obtained numerically. One of them is shown in Fig. 14, which is characterized by the existence of a single Z at which $\theta = 0$ (for all Y). The corresponding I/I_0 vs. X curve for white light has one dark line (propagating with velocity C) and is similar to the of the A_0 soliton (see Fig. 2 of Ref. 2). Estimates of the width and velocity agree with the observed values.[37]

The experimental results of case A above may be understood as follows. At stage 1, $\theta = 0$; at stage 2, $Q > 0$ and a steady state such as that in Fig. 13 is gradually set up; at stage 3, $Q < 0$ and a soliton like that in Fig. 14 is generated which propagates and vanishes at the far end; at stage 4, $Q > 0$ again and a soliton with $\theta \to -\theta$ in Fig. 14 is generated. The orientations of the molecules at each stage in the region $Y > 0$ (in the region $Y < 0$, change θ to $-\theta$) is sketched in Fig. 15a.

Experimental results of cases B and C may be similarly explained (Figs. 15b abd c). Case B is similar to what depicted in Fig. 5. Note that $Q = \text{const}$ in cases A and B. In case C, $Q = Q(X)$ and may be approximated by the step function of $Q = Q_0$ for $X < 0$, $Q = -Q_0$ for $X > 0$, where $Q_0 > 0$ at stages 2 and 4 and $Q_0 < 0$ at stage 3.

Similar results may be obtained in the setup of Fig. 10 by adding a third plate G_3 to the right of G_2 (with the base plate suitably extended). The director equation of motion in this case is (2) or (4) (when boundary effects of glass plates are ignored) and is simpler than (9).

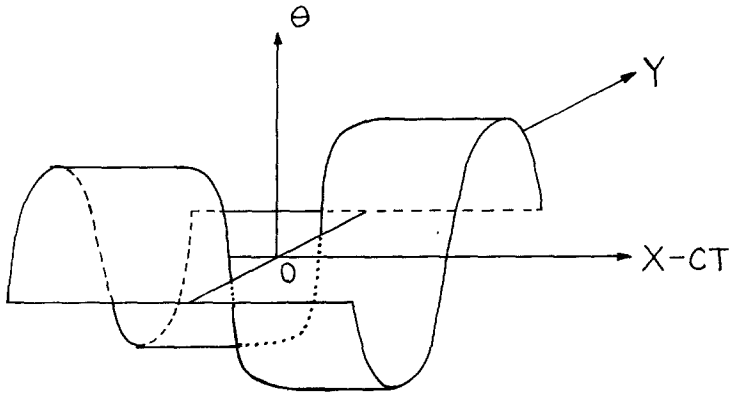

Fig. 14. Numerical soliton solution of Eq. (9), $\theta = \theta(X - CT, Y)$. $Q = \text{const} < 0$.

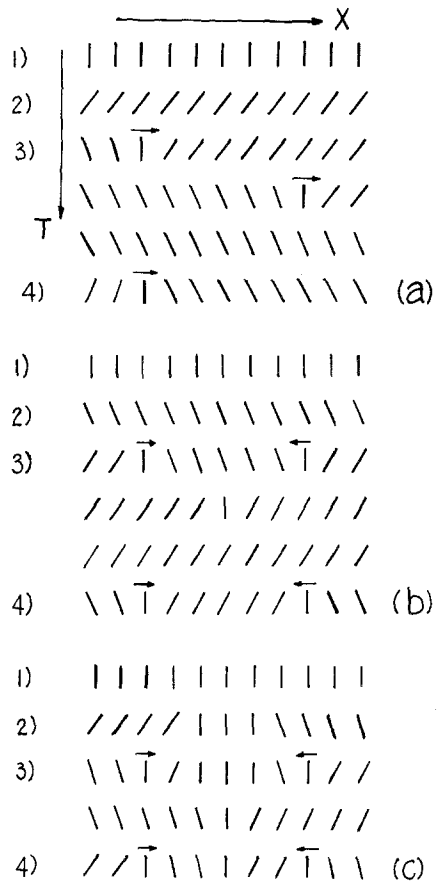

Fig. 15. Molecular orientations (in $Y>0$ region) during the four stages of pressure-gradient experiments described in Fig. 12. Cases (a), (b), and (c) here correspond, respectively, to (a), (b), and (c) of Fig. 12. In the $Y<0$ region, change θ to $-\theta$. The arrows denote the velocities of the solitons (vertical molecules). (a) Single solitons are generated from stage 2) to 3), and from 3) to 4) [but not from 1) to 2)]. (b) Two solitons are generated, collide, and annihilate in 3) [also in 4)]. (c) Two solitons are generated, collide, and merge into one in 3) [and in 4)].

5. AXIALLY SYMMETRIC TWO-DIMENSIONAL SOLITONS

For nematics placed in a cell with circular discs, in general,[20] director angle $\theta = \theta(r, \varphi, z, t)$ where (r, φ, z) are cylindrical coordinates, $\hat{z}$ the normal of the cell, θ the angle between $\mathbf{n}$ and $\hat{z}$. For a thick cell, the z dependence of θ can be ignored. Axial symmetry of the problem eliminates the φ dependence. We then have $\theta = \theta(r, t)$. For torsional shear (in which there is

relative rotation of the two disk[39]), $\mathbf{v} = \omega(z)\, r\hat{\varphi}$ and $\mathbf{n}$ in the $(\hat{\varphi}, \hat{z})$ plane. For radial Poiseuille flow, $\mathbf{v} = [v_0(z)/r]\mathbf{r}$ and $\mathbf{n}$ in the $(\hat{r}, \hat{z})$ plane. In both cases, for r large, the relevant equation of motion is given by[20]

$$K\theta_{rr} - \gamma_1 \theta_t + \tfrac{1}{2}\bar{s}(r)(\gamma_1 - \gamma_2 \cos 2\theta) = 0 \tag{10}$$

where $\bar{s}(r) \equiv \partial v/\partial z$ (and $M \simeq 0$). Note the similarity between (1) and (10). The uniform steady state of (10) is $\pm\theta_0$ (same as in Section 2), irrespective of r. Soliton solutions of (10) do exist. For $\bar{s} > 0$ ($\bar{s} < 0$), $\theta_0(-\theta_0)$ is the stable state.

Experimentally, to generate these solitons in the torsional shear case, one has to split one of the disks into two parts—a small inner disk (of radius r_0) and an outer ring—so that these two parts may be rotated independently of each other with angular frequencies ω_1 and ω_2, respectively, say. [We then have $\omega(z) = \omega_i z$, $\bar{s} = \omega_i r$, $i = 1, 2$, in each region.] This setup is similar to that in Fig. 10. The inner disk corresponds to G_1, the outer ring to G_2, r_0 to X_0, $\omega_i r$ to V_i. We therefore only have to set $\omega_1(t) = \omega_0$, and $\omega_2(t) = \mp\omega_0$ for $t \lessgtr 0$. Under white light (through crossed polarizers), a single dark ring or several dark concentric rings [from more complicated $\omega_1(t)$], corresponding to a single soliton or a multisoliton, may be observed. In principle, these dark rings (like the dark lines in Section 2) may propagate in both inward and outward directions. Alternatively, for technical considerations, one may fix the outer ring and rotate the other (unsplitted) disk instead.

In the radial Poiseulle flow case, one may apply pressure P_1 at the center of the disk by feeding nematics continuously into the center and letting them flow out of the rim in the fashion of Ref. 40. Alternatively, one may seal the outer rim of the disk and allow a ring outlet slightly within the rim. Pressure P_1 at center and P_2 at the ring outlet can then be controlled at will as in Fig. 11 (in which X corresponds to r). The solitons will be observed as dark rings under white light as in the torsional shear case.

6. DISCUSSION

1. In the soliton-bearing shearing nematic and related cases discussed above, the way to generate the solitons may be briefly summarized as follows. For the A soliton (which connects the stable state θ_0 to the unstable state $-\theta_0$) one uses a homeotropic cell and first aligns the molecules in the (uniform) unstable state. At a fixed point in space (usually but not necessarily taken to be near one end of the cell) one then pushes the molecules into the stable state locally and like in the "domino," these molecules will knock down their neighbors in succession. The travel of an

A soliton is the "domino effect" in action. Mathematically, one creates a a localized initial state and let the soliton emerges as time evolves.

The *B* soliton may be excited similarly by using preferably a planar cell (in which molecules at surfaces are parallel to them). There will ne no dark lines under white light in this case because nowhere is $\theta = 0$. However, one may add dyes to the nematic so that the horizontally oriented ($\theta = \pi/2$) nematic molecules will show up distinctively in color. *C* solitons are also excitable but their dimensionless velocity is small and unique (depending only on γ), unlike those of *A* and *B* solitons.

2. The *A* or *B* soliton in shearing nematic is an example of "propagation into an unstable state.[41] In this system the nonlinear equation is the physical equation of motion of real objects (in contrast to the amplitude equations used in pattern-selection problems[26,41]).

These solitons though not linearly stable are nevertheless marginally stable (see Section 2). It seems that their existence and importance in other real physical systems [e.g., the Josephson junction, an atomic monolayer absorbed on a crystal surface, charge density waves, and other systems described by (1)] have been overlooked so far.

As far as nematics are concerned, the experiments discussed in this paper are not mant to be used for measuring the material parameters per se, although this can be done if one so wishes. Rather, they are intended to show and focus one's attention on nonlinear waves in nematics as a subject of study. More important, solitons should play a role in the light scattering spectrum and phase transition properties of nematics under shear. As a system far from equilibrium, shearing nematics is an interesting example from both theoretical and experimental points of view. It is a rare case that one knows how to generate the solitons precisely in a controlled way and to observe them directly and easily. It is especially valuable as a physical system in which one can be observe the evolution of waves in action. The experiments proposed in Sections 2–4 should be performed.

3. In the presence of an external magnetic field $\mathbf{H} = (H_x, H_y, 0)$, an extra term, $\chi_a(H_x \sin\theta + H_y \cos\theta)(H_x \cos\theta - H_y \sin\theta)$, appears on the right-hand side of (1). For electric field **E**, replace **H** by **E** and χ_a by ε_a.[19] When an oscillating external field is used it may be possible to study the chaotic behavior of a shearing nematic similar to that in other systems.[42] The one important parameter γ in (1) (and other equations) may be tuned by varying the temperature, the nematic material itself, or the external (electric or magnetic) field.[19] Note that the various type of solitons in Section 2 no longer exist for $\gamma > 1$ (U no longer has local minimal). Boundary effects of the cell on the soliton properties has been studied.[20]

4. One practical aplication of solitons is in the switching mechanism of chiral smectic liquid crystals.[16] In Ref. 16, an *ad hoc*[43] equation of

motion of the form (1) has been written down. This equation [(1) of Ref. 16], in dimensionless form, is found to be (for $E>0$)

$$\phi_{TT}-\phi_{XX}+\sin\phi=\gamma-\beta\phi_T \tag{11}$$

where $X\equiv z/\lambda$, $T\equiv t/\alpha$, $\lambda\equiv(\theta K/EP)^{1/2}$, $\alpha\equiv(I\theta/EP)^{1/2}$, $\gamma\equiv W/(EP\theta)$, $\beta\equiv\gamma(I\theta EP)^{-1/2}$ (see Ref. 16 for notations). Since[16] $I=\rho\xi^2=4\rho K/EP$, we have $\beta=\gamma(4\rho K\theta)^{-1/2}$, independent of E. For $\gamma=0.1P$, $\rho=1\ \mathrm{g/cm^3}$. $K=2\times10^{-7}$ dyn, $\theta=0.4$,[16] one has $\beta\sim10^2$. Since $\beta\gg1$, the perturbation results of McLaughlin and Scott[44] (for $\gamma\ll1$ and $\beta\ll1$) as adopted in (2) of Ref. 16 in invalid.

To treat the problem properly, let us note that, in analogy to Ref. 45, one can show that for (11) with $\gamma<1$ the velocity of a single soliton, in laboratory units, is

$$u=(\lambda/\alpha)\,\eta(1+\eta^2/\beta^2)^{-1/2} \tag{12}$$

where η is the diminsionless velocity of the soliton. For the C soliton (the one considered in Ref. 45), $\eta=\eta_c(\gamma)$ and is uniquely determined by γ. For A or B solitons, external factors in addition to γ are involved but one always have $\eta<\bar{\eta}=\beta$ (see Table I).

When (12) is applied to the chiral smectic under consideration,

$$u=\tfrac{1}{2}(EP/\rho)^{1/2}\,\eta[1+(4\rho K\theta/\gamma^2)\eta^2]^{-1/2} \tag{13}$$

One sees that $u\propto E^{1/2}$ (a condition presumably required in Ref. 16) if and only if η is independent of E. Such will be the case if the C soliton is the type observed *and* W is proportional to E (so that γ is independent of E). [Note that, in contrast, W is left completely arbitrary in Ref. 16.] The width of the soliton is proportional to λ and hence to $E^{-1/2}$. This point should be checked experimentally, which will help to identify the C soliton.

Note that in (1) of Ref. 16, when the electric field E is reversed in sign, one obtains a *new* equation which is, assuming $W\propto E$ ($E<0$),

$$\phi_{TT}-\phi_{XX}-\sin\phi=-\gamma-\beta\phi_T \tag{14}$$

where E in the definitions of λ, α, γ, and β above should be understood as $|E|$. Equation (14) reduces to (11) under the transformation $\phi\to\pi-\phi$. A C soliton (connecting ϕ_0 to $\phi_0-2\pi$, $0<\phi_0\equiv\sin^{-1}\gamma<\pi/2$) traveling in one direction when $E>0$ is no longer a C soliton (traveling in the opposite direction) for $E<0$. If E changes sign very fast, the former will act as initial state $\phi(X,0)$ in the $E<0$ case and it will take time for it to develop into the latter (connecting $\pi-\phi_0$ to $-\pi-\phi_0$). This evolving time is equal to the product of α and a characteric function of γ and β. Consequently, it is inversely proportional to E.

The switching time τ is the sum of formation time ($\propto E^{-1}$) and the propagation time ($\propto E^{-1/2}$) of the soliton. We therefore have

$$\tau = aE^{-1/2} + bE^{-1} \tag{15}$$

in place of (3) of Ref. 16. (Note that in Fig. 2 of Ref. 16, the experimental dots tend to fall under the straight line at high E.)

ACKNOWLEDGMENTS

One of us (L.L.) thanks A. R. Bishop, G. Doolen, and A. C. Scott for inviting him to the Conference. For useful comments and discussions, he is grateful to A. R. Bishop, H. R. Brand, P. E. Cladis, G. Dee, G. Durand, P. C. Fife, M. D. Kruskal, and R. Pindak. We have benefited from discussions with Feng Kan and Peng Huanwu.

REFERENCES

1. Lin Lei, in *Proceedings of the Conference on Statistical Physics and Condensed Matter Theory, Wuhan, China, 8–14 December 1981* (Huangzhong Inst. Tech. Press, Wuhan, 1982).
2. Lin Lei *et al.*, *Phys. Rev. Lett.* **49**:1335 (1982); **52**:2190(E) (1984).
3. W. Helfrich, *Phys. Rev. Lett.* **21**:1518 (1968).
4. P. G. deGennes, *J. Phys. (Paris)* **32**:789 (1971).
5. F. Brochard, *J. Phys. (Paris)* **33**:607 (1972).
6. L. Leger, *Solid State Commun.* **10**:697 (1972); **11**:1499 (1972); *Mol. Cryst. Liq. Cryst.* **24**:33 (1973).
7. P. E. Cladis and M. Kkeman, *J. Phys. (Paris)* **33**:591 (1972); P. E. Cladis, *Philos. Mag.* **29**:641 (1974).
8. P. E. Cladis and S. Torza, *Colloid Interface Sci.* **6**:487 (1976).
9. R. Ribotta, *Phys. Rev. Lett.* **42**:1212 (1979).
10. J. Prost, in *Liquid Crystals of One- and Two-Diminsional Order*, W. Helfrich and G. Heppke, eds. (Springer-Verlag, Berlin, 1980); in *Symmetries and Broken Symmetries in Condensed Matter Physics*, N. Boccara, ed. (IDSET, Paris, 1981).
11. R. Pindak, C. Y. Yong, R. B. Meyer, and N. A. Clark, *Phys. Rev. Lett.* **45**:1193 (1980).
12. N. A. Clark and S. T. Lagerwall, *Appl. Phys. Lett.* **36**:899 (1980).
13. E. F. Carr and R. W. H. Kozlowski, in *Liquid Crystals*, S. Chandrasekhar, ed. (Heyden, London, 1980).
14. M. Yamashita, H. Kimura, and H. Nakano, *Mol. Cryst. Liq. Cryst.* **68**:79 (1981).
15. M. Yamashita and H. Kimura, *J. Phys. Soc. Jpn.* **51**:2419 (1982).
16. P. E. Cladis, H. R. Brand, and P. L. Finn, *Phys. Rev. A* **28**:512 (1983).
17. A. M. Figueiredo, Ph. Martinot-Lagarde, and G. Durand, *J. Phys. Lett. (Paris)* **45**:L793 (1984).
18. R. Ribotta, A. Joets, and Lin Lei, to be published.
19. Lin Lei and Shu Changqing, *Acta Physica Sinica* **33**:165 (1984) [English translation to appear in *Chinese Phys. (USA)*].

20. Shu Changqing, Ph.D. thesis, Institute of Physics, Chinese Academy of Sciences, Beijing, 1984.
21. Xu Gang, M.Sc. thesis, Institute of Physics, Chinese Academy of Sciences, Beijing, 1984.
22. J. L. Fergason and G. H. Brown, *J. Am. Oil Chem. Soc.* **45**:120 (1968).
23. N. M. Chao and S. H. White, *Mol. Cryst. Liq. Cryst.* **88**:127 (1982).
24. P. C. File, *Mathematical Aspects of Reacting and Diffusing Systems* (Springer-Verlag, Berlin, 1979).
25. K. Uchijama, *J. Math. Kyoto Univ.* **8**:453 (1978).
26. G. Dee and J. S. Langer, *Phys. Rev. Lett.* **50**:383 (1983).
27. G. Ahlers and D. Cannell, *Phys. Rev. Lett.* **50**:1583 (1983).
28. K. Nakajima *et al.*, *J. Appl. Phys.* **45**:3141, 4095 (1974).
29. P. C. Fife and J. B. Mcleod, *Arch. Rat. Mech. Anal.* **75**:281 (1981).
30. D. C. Aronson and H. F. Weinberger, in *Partial Differential Equations*, Lecture Notes in Mathematics, No. 446, J. A. Goldstein, ed. (Springer-Verlag, New York, 1975); *Adv. Math.* **30**:33 (1978).
31. Shu Changqing, Xu Gang, and Lin Lei, *Acta Physica Sinica* (in press).
32. Lin Lei *et al.*, unpublished.
33. Zhu Guozhen, *Phys. Rev. Lett.* **49**:1332 (1982).
34. Xu Gang, Shu Changqing, and Lin Lei, to be published.
35. K. Ko and H. H. Kuehl, *Phys. Rev. Lett.* **40**:233 (1978).
36. Zhu Guozhen, private communication.
37. Shu Changqing, Zhu Guozhen, and Lin Lei, unpublished.
38. Shu Changqing and Lin Lei, paper presented at The Tenth International Liquid Crystal Conference, York, United Kingdom, July 15–21, 1984.
39. He Gang, Shu Changqing, and Lin Lei, paper presented at The Tenth International Liquid Crystal Conference, York, United Kingdom, July 15–21, 1984.
40. K. Hiltrop and F. Fischer, *Z. Naturf.* **31a**:800 (1976).
41. G. Dee, in this issue.
42. H. T. Moon and M. V. Goldman, *Phys. Rev. Lett.* **53**:1821 (1984); A. R. Bishop *et al.*, *Phys. Rev. Lett.* **50**:1095 (1983); M. R. Beasley and B. A. Huberman, *Commun. Solid State Phys.* **10**:155 (1982).
43. P. E. Cladis and H. R. Brand, private communication.
44. D. C. McLaughlin and A. C. Scott, *Phys. Rev. A* **18**:1652 (1978).
45. M. Büttiker and H. Thomas, *Phys. Lett.* **77A**:372 (1980).